

XO-A111 771

AIR FORCE ARMAMENT LAB EGLIN AFB FL F/G 20/4
SUPERSONIC AERODYNAMICS OF A CLASS OF CONE-DERIVED WAVERIDERS (U)
MAY 81 M L RASMUSSEN, D C DANIEL, M C JISCHKE

UNCLASSIFIED

NL

1 OF 1
ASIA
10-11



END
DATE
FILMED
10-82
DTIC

2

SUPERSONIC AERODYNAMICS OF A CLASS
OF CONE-DERIVED WAVERIDERS

Maurice L. Rasmussen
University of Oklahoma, Norman, Oklahoma, and
Air Force Armament Laboratory, Eglin AFB, Florida

Donald C. Daniel
Air Force Armament Laboratory, Eglin AFB, Florida

Martin C. Jischke
University of Oklahoma, Norman, Oklahoma

ABSTRACT

14 MAY 81

The aerodynamic properties of a new class of missile airframes that are derived from the known supersonic flow fields past inclined circular and elliptic cones are discussed. The theoretical foundations and initial force and moment data have been presented recently elsewhere. The present paper advances this knowledge in several ways. Force and moment data for two waverider configurations are presented for $M_\infty = 8$, extending the previous data taken in the range $M_\infty = 3$ to 5. Surface pressure data are also presented, and plans for future free-flight ballistic tests are discussed. The implications of the data and the underlying theory toward the design of highly maneuverable missiles with high lift and low drag, together with proposals for integrated vertical fins and blended inlets, are considered.

INTRODUCTION

Demanding performance and maneuverability requirements for future supersonic and hypersonic missiles will require high-lift, low-drag configurations with good control effectiveness. Non-circular airframe configurations that efficiently integrate volumetric storage, lifting capability, and propulsion components such that aerodynamic heating and radar cross-section are minimized and lift-to-drag ratios are maximized will be required. Discussions of such requirements are given by Giragosian,¹ Fleeman,² and Nielsen.³

A comprehensive research program that addresses many of these requirements is under way. This research is directed toward the study of lifting-body configurations operating at the high Mach numbers of interest. The theoretical analysis is based on small perturbations of axisymmetric flows past circular cones, the perturbations stemming from small angles of attack and small eccentricity of the cone cross section. By this means accurate approximate analytical results are obtained for shock shapes and the shock-layer structure. Since any stream surface can be utilized as a solid surface in an inviscid flow, lifting-body configurations are constructed when free-stream upper surfaces are selected to complement the lower conical-flow stream surfaces.

82 03 09 069

This document has been approved
for public release and its
distribution is unlimited.

I-181

A

AD A111771

DTIC FILE COPY

The resulting aerodynamic shapes are called cone-derived waveriders because they appear to ride on a conical shock wave attached beneath them. The generation of certain specific shapes and the properties of their shock-layer structures are discussed by Rasmussen.⁴ The generalization of this analysis for arbitrary small conical perturbations of a basic axisymmetric conical flow is given by Jischke.⁵ General design considerations relating to the aerodynamic performance of waverider configurations are discussed by Kuchemann.⁶

Experimental results for the forces and moments on two waverider configurations were presented recently⁷ for the Mach-number range 3 to 5, the on-design conditions being $M_\infty = 4$. Those results focused on a configurational comparison of the two waveriders with themselves and with a baseline elliptic cone. For this experimental range, the waverider models were observed to be efficient lift-producing configurations, producing maximum L/D ratios on the order of 2.5 times greater than for the comparative elliptic cone. The overall implications of these results suggest that the waverider configurations make strong contenders for future hypersonic missile and aircraft configurations.

In this paper further results describing the aerodynamics of these waverider configurations are presented. A comparison of the experimental pressure distribution with the theoretical prediction, for the on-design condition $M_\infty = 4$, will be shown. Additional force and moment results for the off-design condition $M_\infty = 8$ will also be presented. Plans for ballistic free-flight tests will be discussed briefly. In view of the promise of these waverider configurations, proposals for integrated vertical fins and blended inlets will be set forth within the framework of the underlying waverider blended-streamsurface philosophy.

DESCRIPTION OF EXPERIMENTS

Sketches of the waverider model configurations that were tested are shown in Figures 1(a) and 1(b) together with a table of the pertinent dimensions in inches. The configuration shown in 1(a) is referred to as the circular-cone waverider (CCWR) and the configuration in 1(b) as the elliptic-cone waverider (ECWR). The base area of the models is denoted by A_b . The position of the body-fixed (or sting) coordinate system, to which the six force and moment coefficients are referred, is also shown. These models were designed on the basis of the theory of Reference 4, and a more complete description of the surface shapes and shock shapes is given in Reference 7. The on-design Mach number is $M_\infty = 4$, for which the theoretical shock shapes are also shown in Figures 1(a) and 1(b).

Tests on the two waverider configurations were conducted in tunnels A and B of the von Karman Facility at the USAF Arnold Engineering Development Center. The tests in tunnel A were conducted over the angle-of-attack and angle-of-sideslip ranges of $\pm 20^\circ$ and at the Mach numbers 3.0, 3.5, 4.0, 4.5, and 5.0, and results for the forces and moments, Schlieren data, and oil-flow data were reported in Reference 7. Corresponding data for $M_\infty = 8$ were obtained in tunnel B. Descriptions of the tunnels and airflow calibration information can be found in Reference 8.

Besides the results described in Reference 7, surface pressure distribution data were obtained in tunnel A. A comprehensive description of these results will be presented in the future. In the present paper only the azimuthal pressure distributions at the on-design conditions ($M_\infty = 4$) will be presented so that a comparison with the related theory can be realized.

The data taken in tunnel B for the nominal Mach number $M_\infty = 8$ (the actual Mach number was $M_\infty = 7.93$) show the effects of strong Mach-number deviations from the on-design conditions. In these tests no measurements of pressure distribution were made. The unit Reynolds number, Re/L , for these tests was 2 million per foot. The corresponding test in tunnel A showed essentially no differences on the force and moment coefficients for the change of unit Reynolds number from 1 to 2 million per foot.

PRESSURE DISTRIBUTIONS

A comparison of theory and experiment for the pressure coefficient on the curved surface of the circular-cone waverider for the on-design conditions ($M_\infty = 4.02$, $\alpha = -3.76^\circ$, $\beta = 0^\circ$) is shown in Figure 2. A corresponding comparison for the elliptic-cone waverider is shown in Figure 3 ($M_\infty = 4.02$, $\alpha = \beta = 0$). The symmetry rays on the curved underneath compression surfaces are denoted by $\phi = 180^\circ$. The theoretical pressure distribution is determined by the perturbation theory described in Reference 7 or 9. The theory agrees with the data well, being most in error near $\phi = 180^\circ$, about 10% for the circular-cone waverider and 5% for the elliptic-cone waverider. For both waveriders the pressure first increases inward from the lip ($\phi = 90^\circ$ for the circular-cone waverider and $\phi = 110^\circ$ for the elliptic-cone waverider), reaches a maximum near the region where the delta winglet fairings into the body, and then decreases toward a minimum at the symmetry ray $\phi = 180^\circ$.

For both configurations it was found that the pressure distributions were conical, that is, the surface pressure on a given ray was constant. Further, the pressure coefficient on the upper flat surfaces was measured to be zero for the on-design condition, in accordance with theory. A comprehensive presentation of the pressure data for the off-design conditions will be forthcoming.

FORCE AND MOMENT COEFFICIENTS

Figures 4 to 11 show the Mach-number variations in the force and rolling-moment coefficients, in the Mach-number range 3 to 8, as either angle of attack or sideslip angle is varied in the range $\pm 20^\circ$. These results are for the forebody contribution only, that is, the contribution of the base pressure has been eliminated. Since $M_\infty = 4$ is the on-design Mach number, $M_\infty = 3$ is the off-design on the low side and $M_\infty = 8$ is the off-design on the high side. Variations in angle of attack or sideslip angle represent off-design conditions due to orientation.

The normal-force coefficients, $C_N \equiv -F_z/qA_b$, are shown in Figures 4 and 5 as functions of angle of attack for the circular-cone and elliptic-cone waveriders. For a given angle of attack, the absolute value of C_N decreases as M_∞ increases. This behavior continues the trend reported in Reference 7

12th May
Barrack

A

for which $M_\infty = 5$ was the largest Mach number. For positive angles of attack the curves for a given Mach number are nearly linear with α up to $\alpha = 20^\circ$. The slopes of those curves yield $C_{N\alpha}$. Approximately, these are, per radian,

<u>CCWR</u>		<u>ECWR</u>	
M_∞	$C_{N\alpha}$	M_∞	$C_{N\alpha}$
3	3.76	3	6.03
4	3.31	4	5.63
8	3.14	8	4.94

As a basis for comparison of these values, the elliptic cone with 1.87 major-minor axis ratio tested in Reference 7 showed values of $C_{N\alpha}$ equal to 2.58 and 1.15 when the cross wind was perpendicular to the major and minor axes, respectively. Of course, $C_{N\alpha}$ for a slender circular cone has the small disturbance value 1.96 approximately. The waveriders, and especially the elliptic-cone waverider, thus produce large normal-force coefficients. The change for above-design Mach numbers is more gradual than for below-design Mach numbers.

The Mach-number effects are small for the axial-force coefficients, $C_A = -F_x/qA_b$, and the drag coefficients, $C_D = D/qA_b$. These results are shown in Figures 6 and 7 for the elliptic-cone waverider. Similar results exist for the circular-cone waverider, and the results for $M_\infty = 4$ can be found in Reference 7. The minimum value of C_D occurs near the angle of zero lift, which has a small, but non-negligible, variation with Mach number.

Variations in the L/D ratios with Mach number and angle of attack are shown in Figures 8 and 9 for the circular-cone and elliptic-cone waveriders. Near its maximum value, L/D decreases as M_∞ increases. This variation with Mach number is most pronounced near the maxima in the curves and is maintained, but to a lessening degree, as α increases. As α decreases from the maximum L/D condition, the variation with Mach number reverses character down to zero lift, the values of L/D increasing as M_∞ increases. As α further decreases such that the lift is negative, a maximum in the absolute value of L/D is reached which is nearly the same value as the maximum L/D value near the on-design condition. Thus the waveriders could fly upside down with the maximum L/D values being nearly the same as for the corresponding near on-design conditions, but the individual values of C_L and C_D would both be less than the near on-design conditions.

The theoretical on-design orientations (at $M_\infty = 4$) are $\alpha = -3.72^\circ$ for the circular-cone waverider and $\alpha = 0$ for the elliptic-cone waverider, and these are very close to the orientation that produces the maximum experimental L/D values. For $M_\infty = 8$, the maximum values of L/D are shifted slightly toward negative angles of attack, and the angles of zero lift become more negative also.

The body-fixed side-force coefficient, $C_y = F_y/qA_b$, as a function of Mach number and sideslip angle, β , is shown in Figure 10 for both the circular-cone and elliptic-cone waveriders. The variation with M_∞ is very

small from $M_\infty = 3$ to 4, that is, near the on-design Mach number. As M_∞ increases from $M_\infty = 4$ to 8, however the value of C_y decreases significantly for a fixed negative value of β .

For sideslip conditions the flow near the leeward and windward lips of the waveriders is different depending on whether the Mach number is below or above the on-design value, which in this case is $M_\infty = 4$. For Mach numbers on-design and below, the shock wave is always detached from the leeward lip, becoming more so as the angle of sideslip increases. For Mach numbers above the on-design value, the shock wave at the leeward lip will remain attached at small sideslip angles and become detached as the sideslip becomes larger. On the other hand, at the windward lip for below-design Mach numbers the shock wave will be detached until a certain sideslip is obtained, and it will be attached as the sideslip further increases. For above-design Mach numbers, the shock wave will remain attached on the windward lip.

The pressure on the surface near the lips of the waveriders appears to be more affected by Mach-number variations than the remainder of the body surface. Since the winglets near the lip are relatively thin, the surface area projected in the direction of the axis is small, and hence the axial and drag coefficients show little variation with M_∞ . The variations of C_N and C_L are much more pronounced, however.

The pitching-moment and yawing-moment coefficients show the corresponding variations with Mach number as their counterpart force coefficients C_N and C_L . Their variations with α and β at $M_\infty = 4$ are shown in Reference 7. The variations of the rolling-moment coefficients, $C_l \equiv M_x / qA_b L$, with Mach number and sideslip angle are shown in Figure 11 for both waveriders. The curves for the circular-cone waverider are nearly linear with sideslip angle and show a small decrease as M_∞ changes from $M_\infty = 3$ to 4, and a much larger decrease as M_∞ changes further from $M_\infty = 4$ to 8. For the elliptic-cone waverider, the curves for $M_\infty = 3$ and 4 show some nonlinearity with sideslip angle, and for larger amounts of sideslip C_l decreases more as M_∞ increases from $M_\infty = 3$ to 4 than it does from $M_\infty = 4$ to 8. The rolling-moment coefficient is much larger for the circular-cone waverider, and it appears that both waveriders would tend to roll into a turn when $\alpha = 0$.

PLANNED BALLISTIC TESTS

Plans have been formed for ballistic free-flight tests of the elliptic-cone waverider at the Air Force Armament Laboratory Aeroballistic Research Facility. These tests are meant to determine static and dynamic stability characteristics of the elliptic-cone waverider and to observe its overall flight behavior. The model will be approximately $L = 2.5$ inches long and launched at about $M_\infty = 3$, which is the maximum speed available for this model at this facility. For a homogenous cone the center of mass occurs at 75% of its length from the vertex. For the elliptic-cone waverider, the forebody center of pressure is at approximately 68% of the length from the vertex in the pitching mode and 82% of the length of the cone in the yawing mode (based on the data of Reference 7). In order to obtain static stability, the model will be hollowed out by drilling into the base so that the center of mass is forward of the center of pressure.

CONSIDERATIONS ON THE DESIGN OF FINS AND INLETS

The cone-derived waveriders produce large lifting forces and L/D ratios which are favorable for missile maneuverability and range. The on-design conditions can be predicted well by the underlying, relatively simple, perturbation theory. This is very desirable as a design tool, yielding conceptual simplicity and allowing for ease of parametric studies. The experimental study shows that off-design effects resulting from Mach-number variation and orientation of the body produce flows that remain clean and essentially conical, without undesirable secondary flow or other effects. The data together with the theory show substantial promise for the design of practical new missile configurations. Toward these ends, it is useful to speculate on the design of control surfaces and blended-inlet configurations.

VERTICAL FINS

It is conceivable that control devices such as flaps and ailerons can be built into the trailing edges of either the flat upper surfaces or the curved lower surface of the waveriders. It is also possible that a vertical fin would be desirable or necessary for proper control. A fin that produces a known simple disturbance flow field can be designed. Reference 4 suggests a methodology for doing this by means of well-known caret-waverider configurations which are constructed from the known two-dimensional constant flow behind plane oblique shock waves. Two such caret-waverider vertical fins are shown attached to an elliptic-cone waverider in Figures 12(a) and 12(b). The fin in Figure 12(a) begins at the vertex of the elliptic-cone waverider, and the fin in Figure 12(b) begins at half the distance back on the body. For the purposes of illustration, these fins are shown thicker than probably desirable. The starting position of the fin and the thickness of the fin at its base (described by a wedge flow-disturbance angle) allow for versatility in the design of this family of fins. For on-design conditions, the shock produced by this fin is planar, and the flow behind it is uniform and known. Thus further flow disturbances produced by flaps on the trailing edge of the fin can be calculated. Experimental tests are being planned for a set of such fins attached to the elliptic-cone waverider.

INLETS

The geometrical surfaces of waveriders are constructed by utilizing the stream surfaces of known flow fields. In a sense, therefore, viscous effects ignored, these waverider surfaces are natural surfaces and the flow tends to move easily past them. This motion appears to be substantiated by the data presented herein and in Reference 7. In addition, the flow properties for the waverider configurations are known for the special on-design condition. It is useful to extend this concept to the design of exterior contours of inlets. The basic ideas can be formulated by constructing an idealized conical waverider with an inlet.

If $\vec{V}(\vec{r})$ is a known velocity field and $d\vec{r}$ is a differential line element, then the differential equation for a streamline element is given by $\vec{V} \times d\vec{r} = 0$. In spherical coordinates and for conical flow, this reduces to⁴

$$\frac{dr}{u(\theta, \phi)} = \frac{rd\theta}{v(\theta, \phi)} = \frac{r \sin \theta d\phi}{w(\theta, \phi)}, \quad (1)$$

where u , v , and w are the known radial, polar, and azimuthal components of velocity. The last two members of Equation (1) are independent of r and integration thus yields the form

$$F_1(\theta, \phi) = C_1, \quad (2)$$

where C_1 is an arbitrary constant of integration. In the framework of perturbation theory, the lowest order of approximation of Equation (2) was used to generate the curved surfaces of the circular-cone and elliptic-cone waveriders.⁴

The first two members of Equation (1) can be written as

$$\frac{dr}{r} = \frac{u(\theta, \phi)d\theta}{v(\theta, \phi)}. \quad (3)$$

When ϕ is eliminated in Equation (3) in favor of θ by means of Equation (2), then Equation (3) can be integrated in principle to the form

$$F_2(r, \theta; C_1) = C_2, \quad (4)$$

where C_2 is another arbitrary constant of integration. Equations (2) and (4) constitute two families of stream surfaces, and their intersections produce the streamlines, a specific value of C_1 and C_2 for each streamline.

Any arbitrary stream surface is described by $F(\vec{r}) = 0$, where

$$\vec{V} \cdot \nabla F = 0 \quad \text{on} \quad F = 0. \quad (5)$$

Equation (5) is a first-order equation for $F(\vec{r})$, and it has the characteristic equations (1). Thus any arbitrary function of the constants of integration C_1 and C_2 is a solution to Equation (5), that is,

$$F = F(C_1, C_2). \quad (6)$$

It follows that an arbitrary stream surface can be specified by setting one constant of integration to be an arbitrary function of the other:

$$C_2 = G(C_1). \quad (7)$$

Since the functional relations (2) and (4) are presumed known, any arbitrary stream surface can be developed by means of Equation (7).

These ideas can be developed simply for an idealized conical waverider, devised from the well-known axisymmetric flow past a circular cone. In this case, we have $u = u_0(\theta)$, $v = v_0(\theta)$, and $w = 0$. Equation (2) becomes simply

$$\phi = C_1, \quad (8)$$

that is, any plane through the axis of symmetry is a stream surface. It is also possible to integrate Equation (3) to the form

$$r [\rho_0(\theta)v_0(\theta)\sin\theta]^{\frac{1}{2}} = C_2, \quad (9)$$

where $\rho_0(\theta)$ is the density field for the axisymmetric cone flow. For hypersonic flow past slender cones,⁴ the density field is nearly a constant, and Equation (9) can be approximated by the form

$$r [\theta^2 - \delta^2]^{\frac{1}{2}} = C_2, \quad (10)$$

where δ is the semi-vertex angle of the cone. Setting $C_2 = 0$ yields $\theta = \delta$, which is the stream surface for the cone itself. Any arbitrary stream surface can be generated by the equation

$$r [\rho_0(\theta)v_0(\theta)\sin\theta]^{\frac{1}{2}} = G(\phi), \quad (11)$$

where $G(\phi)$ is an arbitrary function.

Figures 13(a), (b), and (c) show the development of an idealized conical waverider with an inlet. We arbitrarily construct the exterior contour of the inlet to be axisymmetric by choosing the function $G(\phi)$ to be a constant, so that Equation (9) or its approximation Equation (10) holds. Setting $C_2 = 0$ yields the surface of the cone itself. Another positive value of $C_2 = C_2^*$ yields an exterior stream surface shown in Figure 13(a). The flow in the cylinder in front of shock contained by this axisymmetric stream surface passes through an annular region embracing the basic-cone body, $\theta = \delta$. The thickness of this annular region goes to zero as r goes to infinity. An ideal axisymmetric inlet is constructed by treating the stream surface C_2^* as a solid surface starting at some arbitrary distance behind the shock, as shown in Figure 13(b). The flow in the original cylinder ahead of the shock thus passes through the annular region which is now the inlet. The flow outside the original cylinder passes around the inlet which is now the exterior of the body. In this idealized inviscid flow, the inlet has a sharp lip that allows the flow to pass around it without the formation of a shock, providing that the internal flow can be appropriately accommodated or completely swallowed. An idealized conical waverider configuration can now be constructed by using the family of stream surfaces $\phi = C_1$ to form delta winglets of infinitesimal thickness. Thus, a lower portion of Figure 13(b) is used to construct the idealized conical waverider in Figure 13(c).

A similar procedure can be used to construct inlets for the circular-cone and elliptic-cone waveriders shown in Figure 1. A study is now under way making use of perturbation methods in accordance with the original analysis.

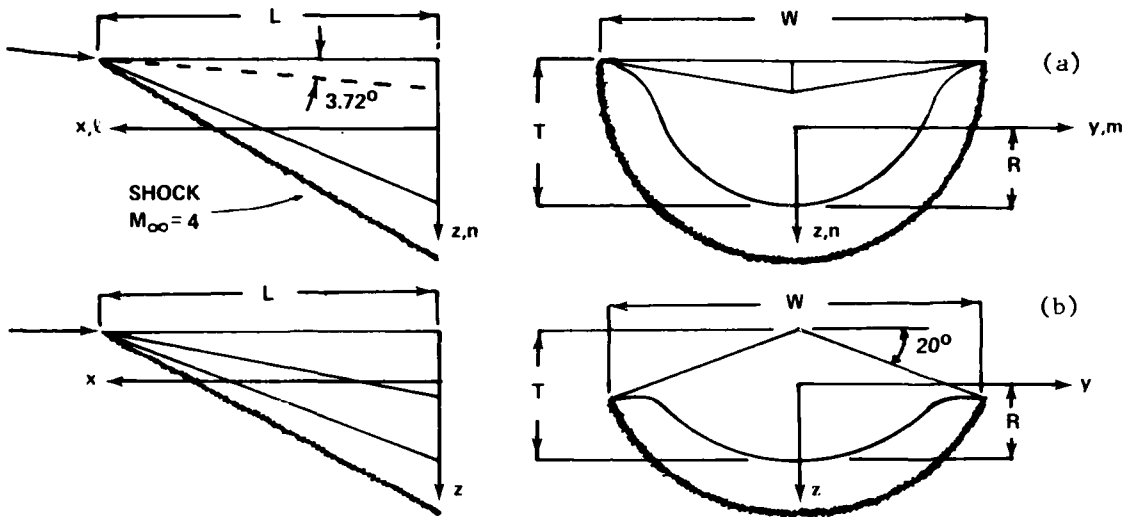
It is desired to shape the external boundary of the inlet so that it blends into the curved undersurface of the basic waverider. In this way sharp corners do not appear in the final contour of the waverider undersurface. Since no shock appears from the lip of the inlet in the ideal-flow on-design case, the inlet does not produce wave drag as it would in other arbitrary designs. Wind tunnel tests are being planned for an inlet added to the elliptic-cone waverider to ascertain the flow properties of on-design and off-design conditions in a real flow.

CONCLUDING REMARKS

The basic theory and supportative data base for the cone-derived waveriders discussed herein make these lifting-body configurations attractive for meeting the high-speed, high-performance requirements of present-day missile technology. Further studies on fins and inlets will add to the technology base of these novel configurations. In this connection other studies under way include contour optimization and boundary-layer development.

REFERENCES

1. Giragosian, P. A., "Critical Aerodynamic Technology Issues in Air-to-Air Missile Design," AIAA Paper 79-0089, presented at AIAA 17th Aerospace Sciences Meeting, New Orleans LA, January 1979.
2. Fleeman, E. L., "Aeromechanics Technologies for Tactical and Strategic Guided Missiles," presented at the AGARD FMP Meeting on Missile Systems Flight Mechanics, London, England, May 1979.
3. Nielsen, J. N., "Missile Aerodynamics - Past, Present, Future," AIAA Paper 79-1819 (Wright Brothers Lectureship in Aeronautics), presented at the AIAA Aircraft Systems and Technology Meeting, New York, August 1979.
4. Rasmussen, M. L., "Waverider Configurations Derived from Inclined Circular and Elliptic Cones," *J. of Spacecraft and Rockets*, Vol. 17, No. 6, Nov. - Dec. 1980, pp. 537-545.
5. Jischke, M. C., "Supersonic Flow Past Conical Bodies with Nearly Circular Cross Sections," *AIAA Journal*, Vol. 19, No. 2, February 1981, pp. 242-245.
6. Küchemann, D., The Aerodynamic Design of Aircraft, Pergamon Press, London, Chap. 8, 1978.
7. Rasmussen, M. L., Jischke, M. C., and Daniel, D. C., "Experimental Results for Forces and Moments on Cone-Derived Waveriders in the Mach-Number Range 3 to 5," AIAA Paper 81-0149, AIAA 19th Aerospace Sciences Meeting, St. Louis, January 1981.
8. Test Facilities Handbook (Eleventh Edition), "Von Karman Gas Dynamics Facility," Vol. 3, Arnold Engineering Development Center, Arnold Air Force Station, Tennessee, June 1979.
9. Rasmussen, M. L., and Lee, H. M., "Approximation for Hypersonic Flow Past a Slender Elliptic Cone," AIAA 17th Aerospace Sciences Meeting, New Orleans, January 1979.



Model Dimensions (inches)

	L	W	T	R	A_b in. ²
Circular-Cone Waverider	23.62	21.98	7.96	4.46	103.60
Elliptic-Cone Waverider	23.62	21.50	7.11	4.62	75.83

Figure 1. Model Configurations: (a) Circular-Cone Waverider (CCWR), (b) Elliptic-Cone Waverider (ECWR).

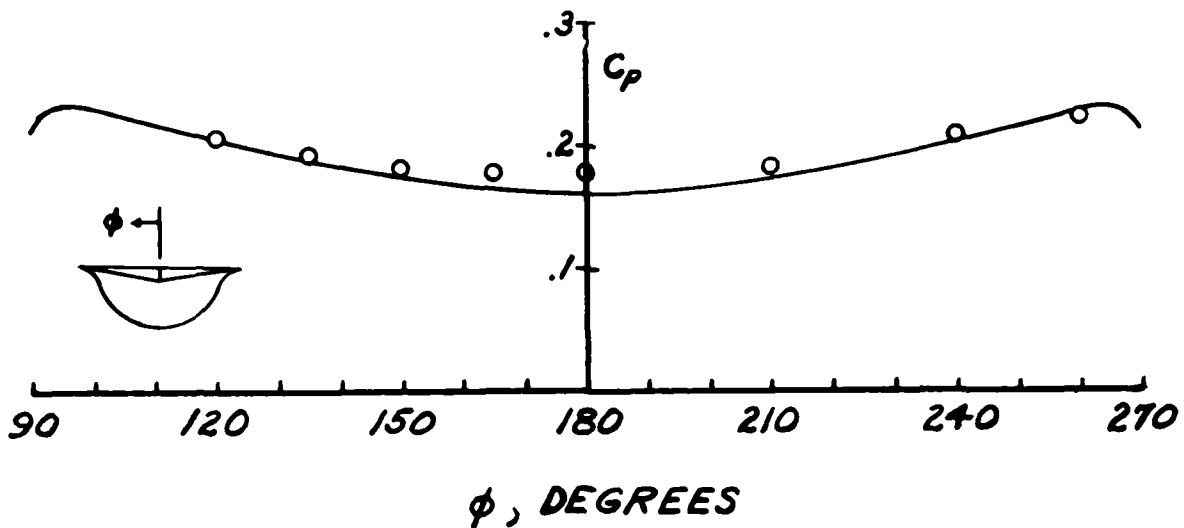


Figure 2. Comparison of Theory and Experiment of Under-surface Pressure Coefficient for Circular-Cone Waverider: On-design Conditions, $\alpha = -3.76^\circ$, $\beta = 0$, $M_\infty = 4.02$.

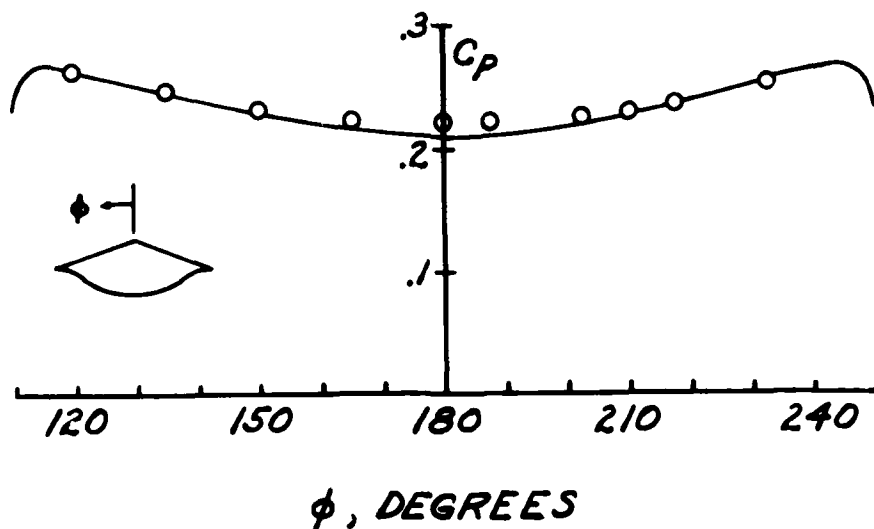


Figure 3. Comparison of Theory and Experiment of Under-surface Pressure Coefficient for Elliptic-Cone Waverider: On-design Conditions, $\alpha = \beta = 0$, $M_\infty = 4.02$.

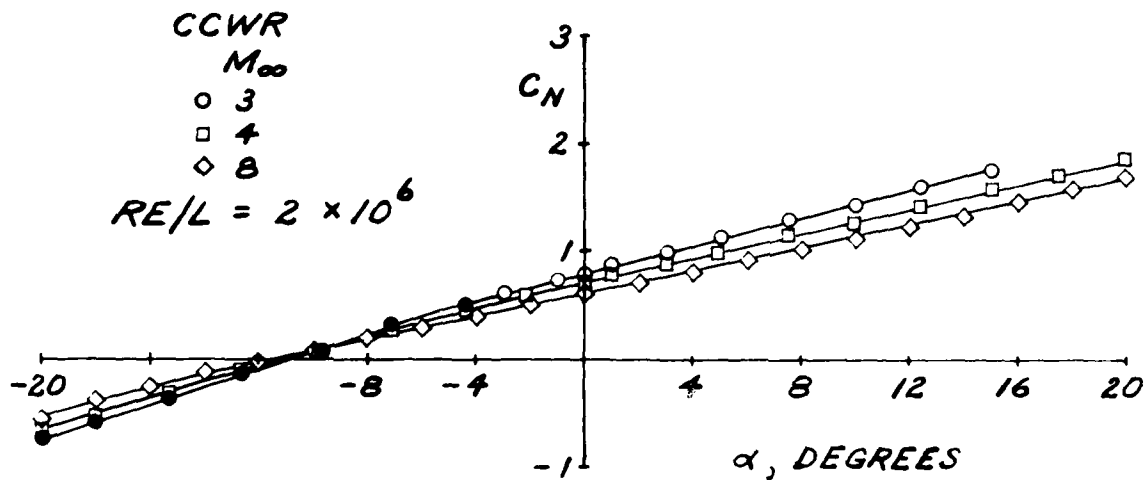


Figure 4. Normal-Force Coefficient versus Angle of Attack for Circular-Cone Waverider at Different Mach Numbers. Solid Symbols Represent $Re/L = 10^6$.

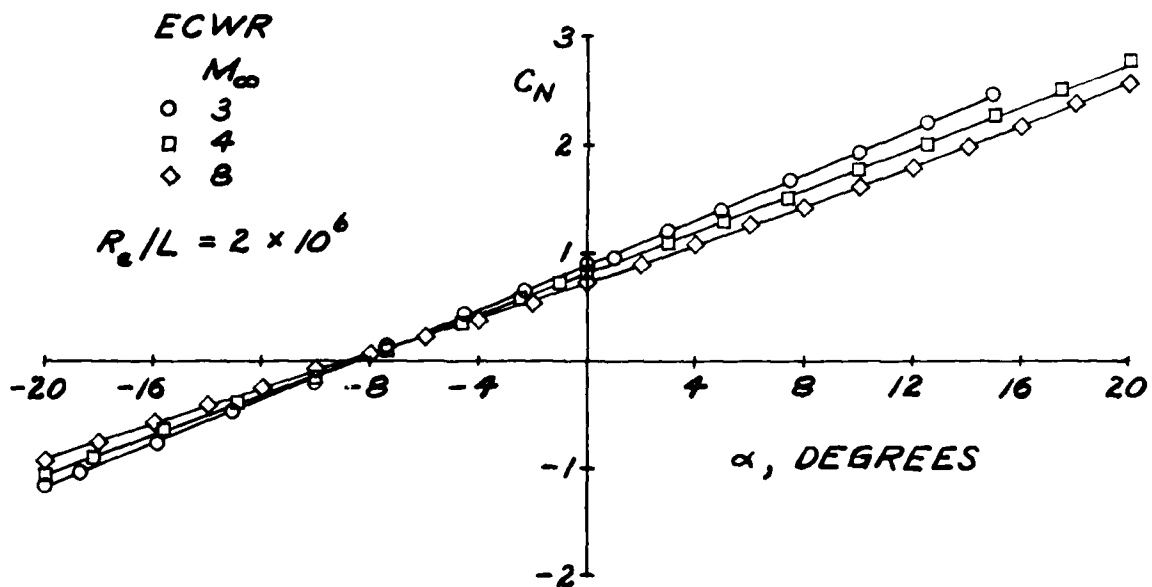


Figure 5. Normal-Force Coefficient versus Angle of Attack for Elliptic-Cone Waverider at Different Mach Numbers.

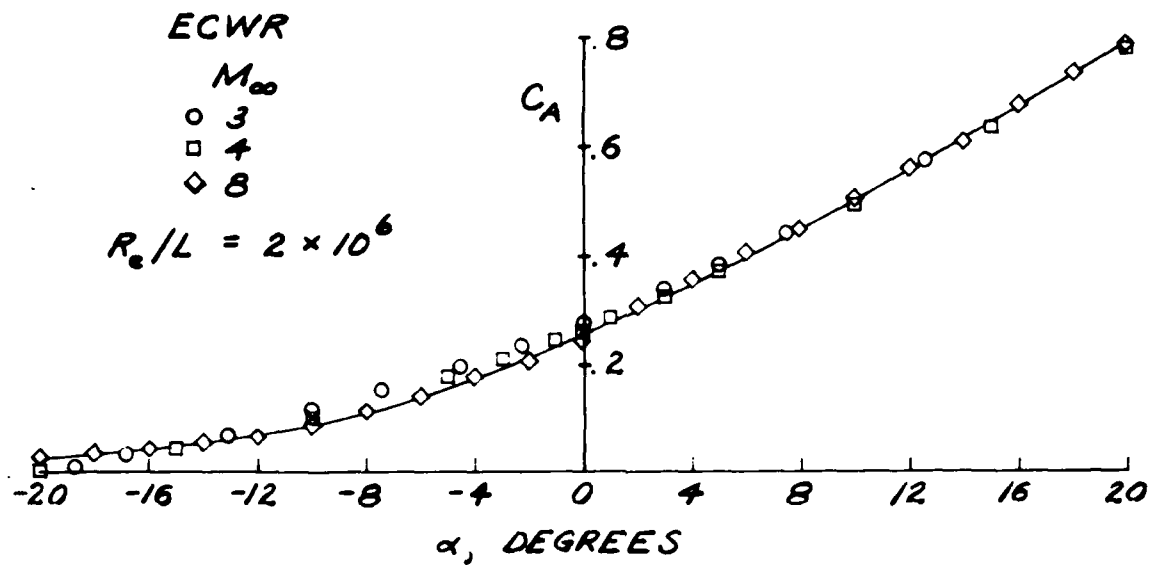


Figure 6. Axial-Force Coefficient versus Angle of Attack for Elliptic-Cone Waverider at Different Mach Numbers.

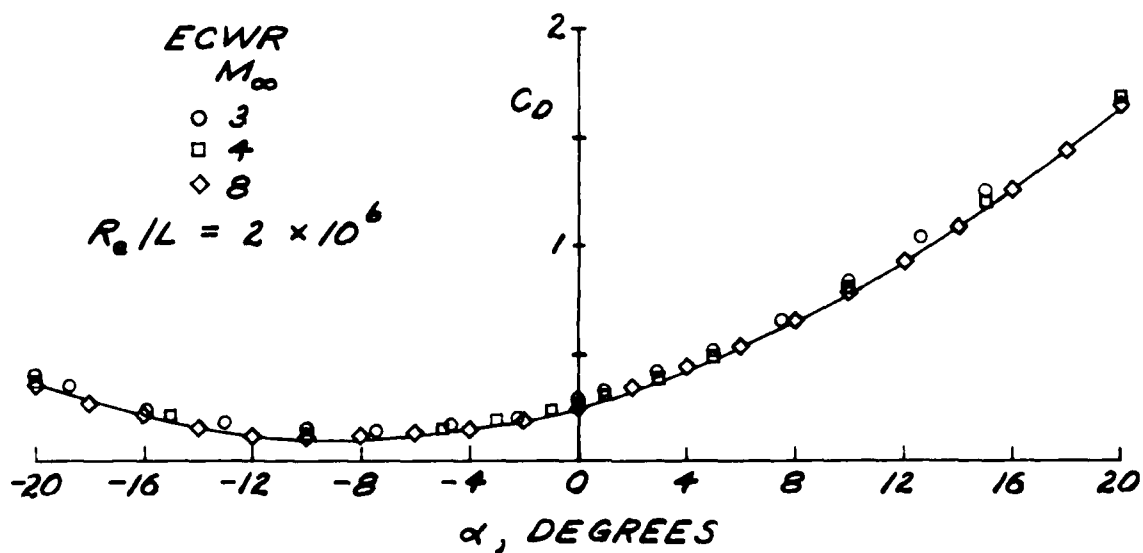


Figure 7. Drag Coefficient versus Angle of Attack for Elliptic-Cone Waverider at Different Mach Numbers.

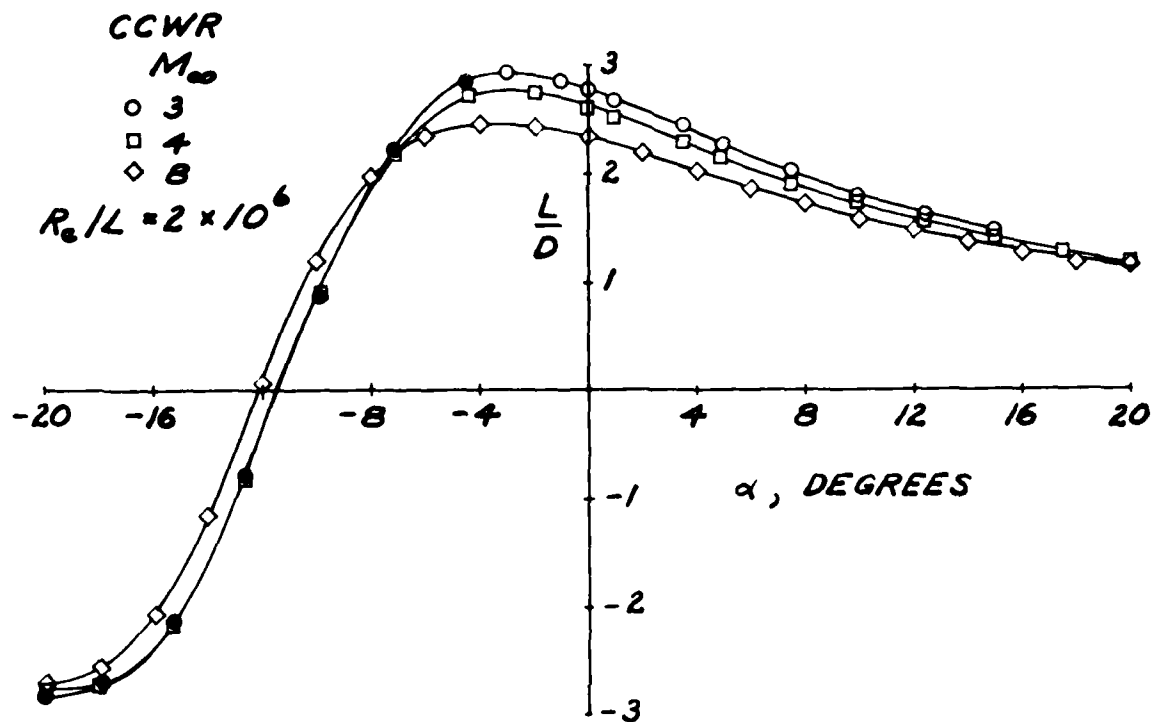


Figure 8. L/D Ratio versus Angle of Attack for Circular-Cone Waverider at Different Mach Numbers. Solid Symbols Represent $Re/L = 10^6$.

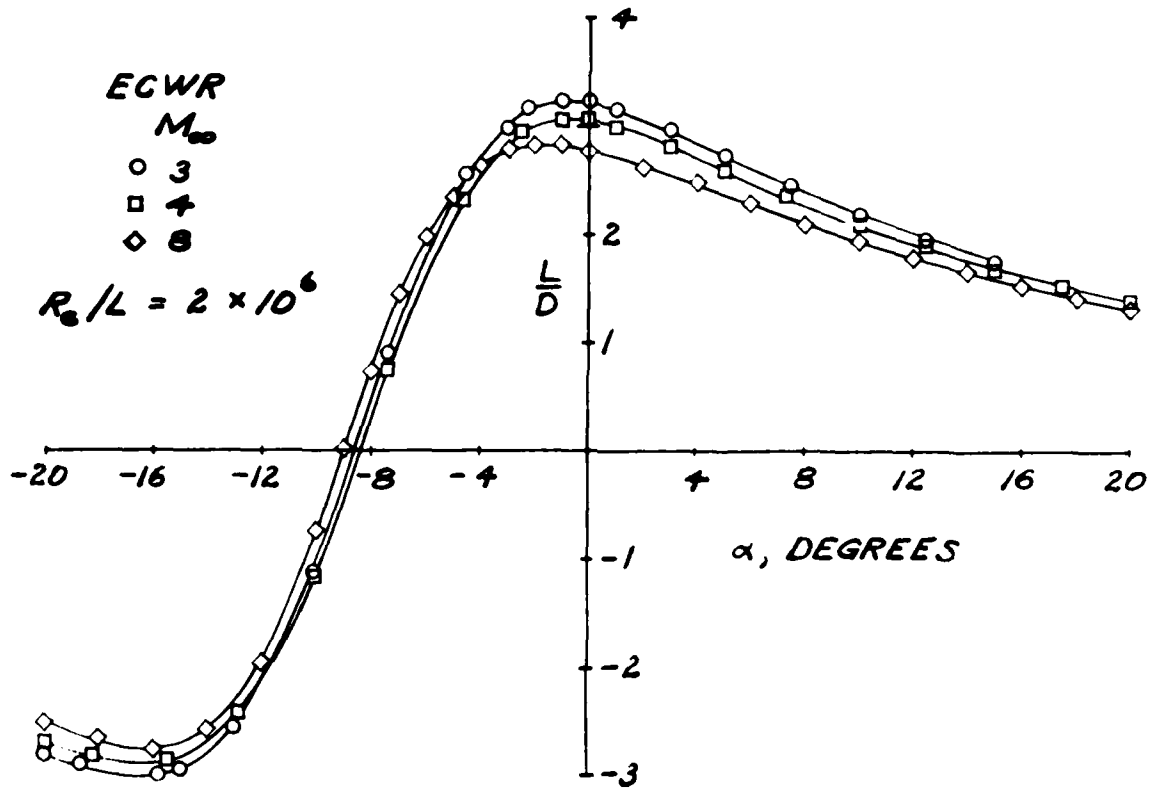


Figure 9. L/D Ratio versus Angle of Attack for Elliptic-Cone Waverider at Different Mach Numbers.

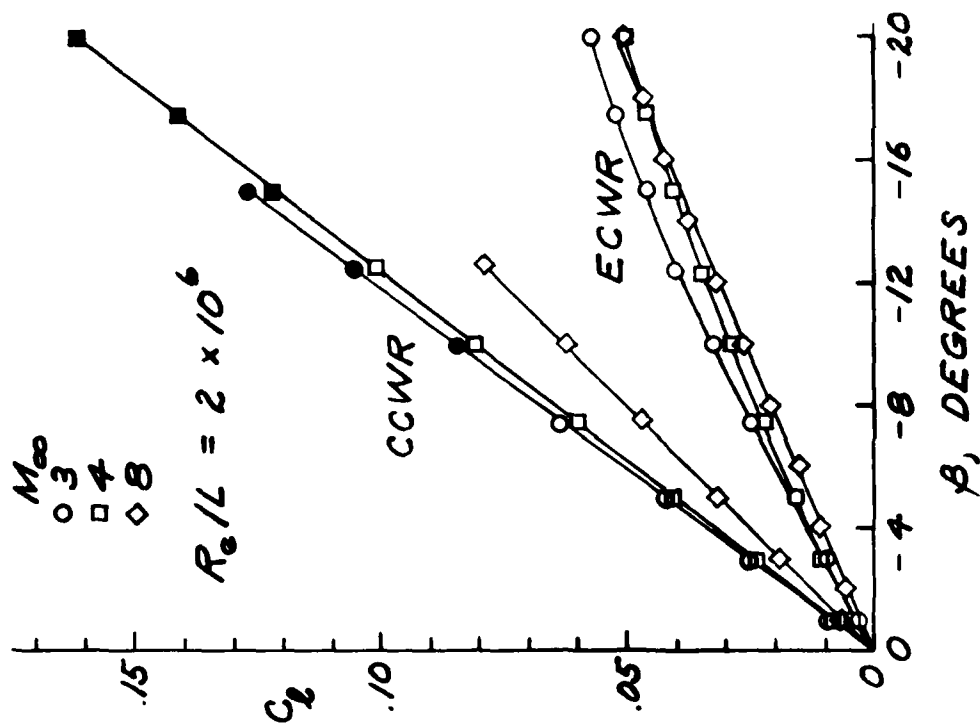


Figure 11. Rolling-Moment Coefficient versus Angle of Sideslip for Different Mach Numbers. Solid Symbols Represent $Re/L = 10^6$.

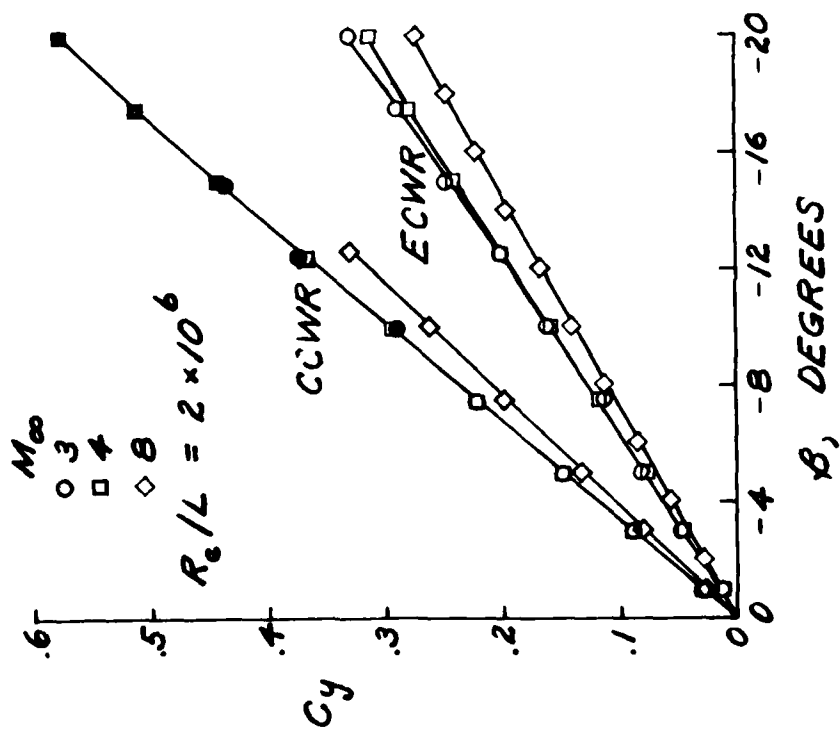


Figure 10. Side-Force Coefficient versus Angle of Sideslip for Different Mach Numbers. Solid Symbols Represent $Re/L = 10^6$.

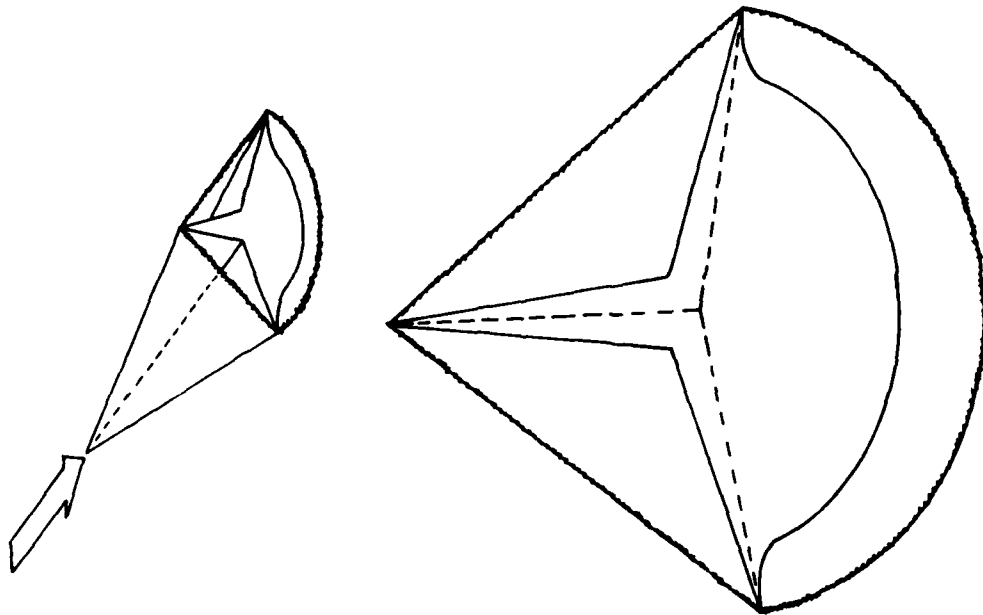


Figure 12(a) Vertical Fin Starting at Vertex of an Elliptic-Cone Waverider.

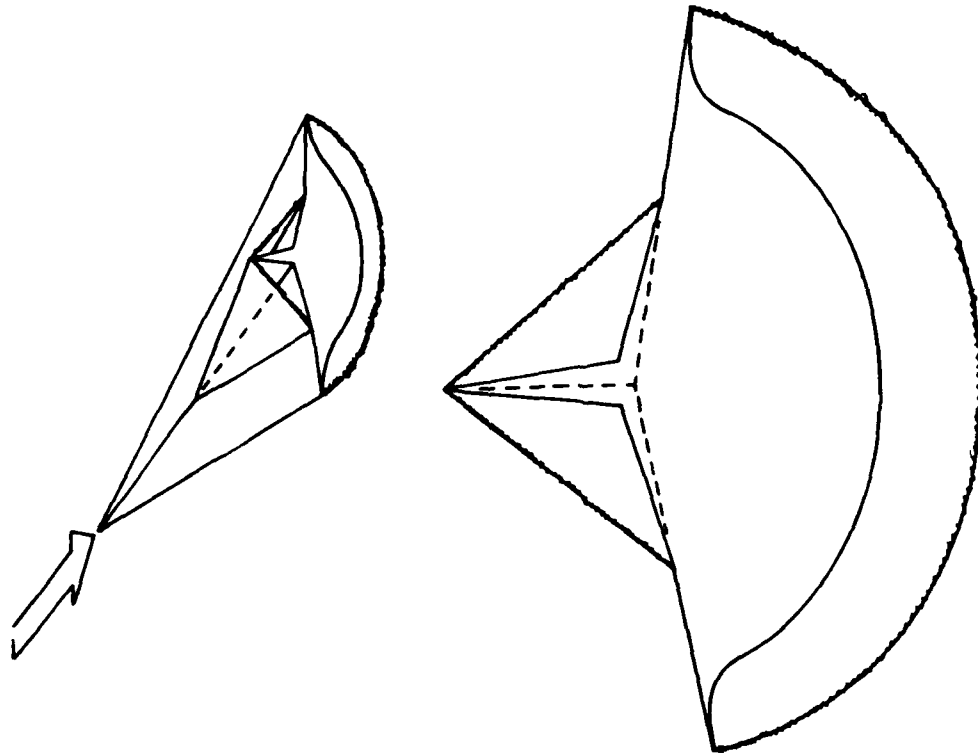


Figure 12(b). Vertical Fin Starting at Half Length of an Elliptic-Cone Waverider.

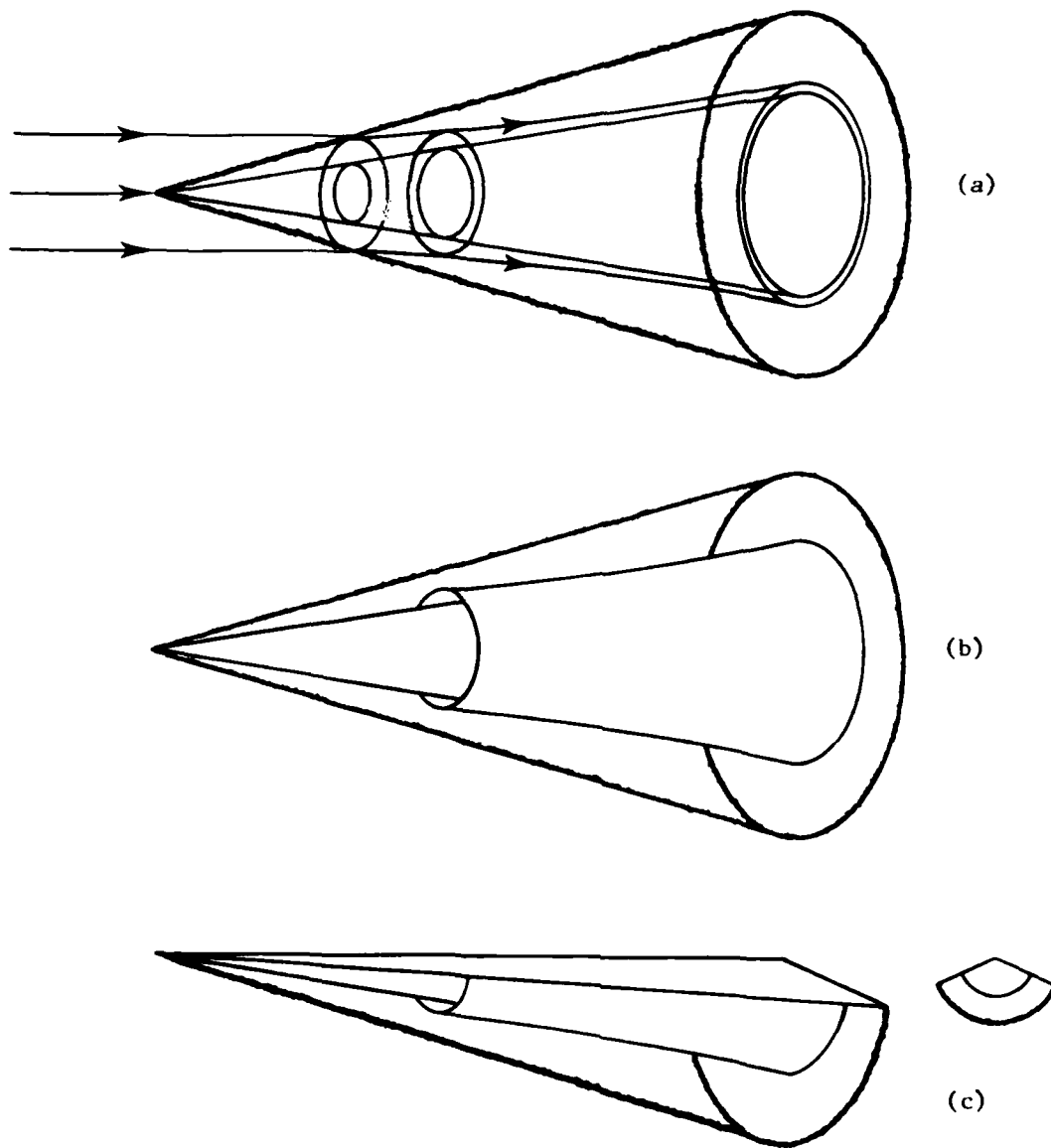


Figure 13. Construction of Axisymmetric Inlet on Idealized Conical Waverider: (a) Axisymmetric Stream Surfaces in Axisymmetric Flow Past a Circular Cone, (b) Axisymmetric Inlet on Circular Cone, (c) Axisymmetric Inlet on Idealized Conical Waverider.

TE
ED
82